

Anisotropy in the Microwave Sky at 90 GHz: Results From Python II

J. E. Ruhl^{1,2}, M. Dragovan^{1,3}, S. R. Platt⁴, J. Kovac⁵, and G. Novak⁶

Received _____; accepted _____

¹Enrico Fermi Institute, Univ. of Chicago, Chicago, IL 60637

²Current address: Dept. of Physics, Univ. of Calif. Santa Barbara, Santa Barbara, CA 93106

³Dept. of Astronomy and Astrophysics, Univ. of Chicago, Chicago, IL 60637

⁴Yerkes Observatory, Univ. of Chicago, Williams Bay, WI 53191

⁵Dept. of Physics, Princeton Univ., Princeton, NJ 08544

⁶Dept. of Physics and Astronomy, Northwestern Univ., Evanston, IL 60208

ABSTRACT

We report on additional observations of degree scale anisotropy at 90 GHz from the Amundsen-Scott South Pole Station in Antarctica. Observations during the first season with the Python instrument yielded a statistically significant sky signal with an amplitude of $\Delta T/T \sim 3.5 \times 10^{-5}$ for a Gaussian autocorrelation function model with a coherence angle $\theta_c = 1^\circ$. In this paper we report the confirmation of that signal with data taken in the second year, and on results from an interleaving set of fields. Using the entire data set, we find $\Delta T/T = \sqrt{C_0} = 2.8_{-0.7}^{+1.1} \times 10^{-5}$ for the Gaussian autocorrelation model mentioned above, and $\Delta T/T = \sqrt{\ell_e(\ell_e + 1)C_\ell/(2\pi)} = 2.1_{-0.5}^{+0.7} \times 10^{-5}$ for a band-power estimate, where $\ell_e = 93$ is the effective center of our window function. The stated errors represent a 68% confidence interval in the likelihood added in quadrature with a 20% calibration uncertainty.

Subject headings: cosmic microwave background — cosmology: observations

1. Introduction

Anisotropies in the Cosmic Microwave Background Radiation (CMBR) contain a wealth of information about the conditions and processes that led to the formation of large scale structures in the universe. Whether the correct model of the evolution of the universe involves baryons, exotic cold dark matter, massive neutrinos, topological defects, a standard ionization history or reionization at a modest redshift, the content and history of the universe affect the observed anisotropies of the CMBR (see White, Scott and Silk (1994) for a review). Constrained by the measured level of anisotropy on large angular scales (Bennett *et al.* 1994, Ganga *et al.* 1993), different models predict varying levels of anisotropy on smaller scales. Several observing teams (Cheng *et al.* 1994, de Bernardis *et al.* 1994, Devlin *et al.* 1994, Gundersen *et al.* 1995, Netterfield *et al.* 1995) including our own have reported detections of anisotropy on angular scales near 1° . Improvements in these measurements should help discriminate between the current models of large scale structure formation.

The Python instrument is designed to search for anisotropies at an angular scale near 1° . The first observations (hereafter PyI) with Python were made between 1 and 15 January 1993 at the Amundsen-Scott South Pole station (Dragovan *et al.* 1994, hereafter Paper I). Statistically significant signals were detected in observations at high Galactic latitude ($|b| > 49^\circ$).

We report here the results of a second set of observations (hereafter PyII), made between 12 and 23 December 1993 from the same site. The bulk of the observing time in the second season was spent on the PyI field (“Field A”), in an effort to repeat that measurement. The remainder was spent on a set of interleaving spots (“Field B”). The observation of the Field A spots serves as a further check for the effects of interfering signals that would differ from one year to the next, including effects from atmospheric emission, cosmic ray hits in the bolometers, and radiofrequency interference. Additionally, the Sun was approximately 20° further away from the observed fields during the PyII season than it was for PyI.

2. Instrument

The Python instrument (Paper I, Ruhl 1993) consists of a 0.75 m diameter off-axis parabolic telescope that couples radiation into a 2×2 array of bolometric detectors. The beam response is well approximated by a Gaussian with a full width at half maximum

of $(0.75 \pm 0.05)^\circ$. Radiation from the sky is first reflected off a vertical flat before being focused into the cryostat by the primary. Rotation of the flat about a vertical axis moves the detector response horizontally across the sky. The telescope is mounted on an azimuth-elevation mount and is surrounded by a large shield that protects the instrument from being illuminated by the Sun or Earth.

Inside the cryostat there are four corrugated feed horns at the focal plane of the primary. Radiation that enters a feed horn passes through a set of single-mode waveguide filters that define the passband at $\lambda = 3.3$ mm before reaching the bolometric detectors. The detectors use a layer of bismuth evaporated on a diamond wafer as the absorbing element, and a chip of neutron transmutation doped germanium as the thermistor element. They are operated at 50 mK, cooled by a ^3He guarded adiabatic demagnetization refrigerator (Ruhl & Dragovan 1992). An additional bolometer (the “dark channel”), mounted on the cold stage but kept in a sealed cavity, acts as a monitor for extraneous pickup.

New bolometers, constructed using the same methods as the originals, were installed for the PyII observing season. However, two of the four new optical channels did not work well. One channel was a factor of 3 less sensitive than typical ($6 \text{ mK}\cdot\sqrt{\text{s}}$ instead of $2 \text{ mK}\cdot\sqrt{\text{s}}$); the other was unusable due to an electrical problem in the dewar. Fortunately, one good channel was on the upper row, and the other was on the lower, making possible the confirmation of the bulk of the PyI data.

The two most significant changes to the telescope between PyI and PyII were the improved balancing of the chopping mechanism for the external switching flat, and the installation of a microwave-absorbing guard ring around the primary.

3. Observations

The Sun, Moon, and two sources in the Carinae nebula were used as absolute pointing references each season; additionally, Venus was used during the PyI season. We estimate our absolute pointing accuracy to be $\pm 0.1^\circ$ each year, or $\pm 0.15^\circ$ for the relative pointing accuracy of the PyI and PyII datasets.

The same observing strategy was used for PyI and PyII, and is described in Paper I. The combination of a fast 3-beam chop (2.5 Hz full cycle) and slower beamswitching (10 to 30 seconds per position) yields a 4-beam response on the sky,

$$\Delta T_j^k = -\frac{1}{4}T_j + \frac{3}{4}T_{j+1} - \frac{3}{4}T_{j+2} + \frac{1}{4}T_{j+3}, \quad (1)$$

where the T_j 's are the antenna temperatures of patches on the sky separated by 2.75° along a horizontal line. A scan consists of measuring ΔT_j^k three times successively ($k = 1, 2, 3$) at each of 7 positions j on the sky. The left and right hand channels in a given row of the array measure many of the same 4-beam patterns; the spots measured by the left hand side are given by $j = 1, \dots, 7$, while those made by the right correspond to $j = 2, \dots, 8$.

The time-ordering of the right and left-hand 3-beam measurements (“stares”) are reversed from one value of j to the next. For the first 4-beam pattern ($j = 1$ for the left channels, $j = 2$ for the right), the left stare is measured first. For the second 4-beam pattern the right stare is measured first, and so on. This causes a drifting 3-beam offset to appear as an oscillating 4-beam signal on the sky. However, the measured linear drifts in the 3-beam offset within each scan are both small and symmetric about zero, making this effect unimportant. The average 3-beam offsets are less than 1 mK for all the PyI and PyII channels, and the average slopes are within 2σ of zero, with an error of $\sigma \sim 1\mu\text{K}/\text{stare}$.

4. Calibration

The PyI observations were calibrated by a combination of elevation scans and the placement of known-temperature blackbody and low emissivity foam loads in the optical path, as described in Paper I and Ruhl *et al.* 1995. The PyII observations were calibrated using the foam loads; the loads were in turn calibrated by placing a large liquid-nitrogen-cooled load beneath the dewar and alternately switching the foam and two known-temperature loads into the optical path. This calibration of the foam loads was done *in situ* on the telescope during the PyII season, rather than in a 300 K room, reducing possible systematic effects in the measurement. The DC gain measured using the foam loads was converted to an AC gain by comparing the signals seen while switching on and off a foam load slowly (0.1 Hz) with those seen while switching at the frequency used for the observations (5 Hz).

The relative calibrations of the various bolometer channels (four channels for PyI, three for PyII) were checked using two sources in the Carinae nebula; the results from all seven channels lie within 15% of the average. The two sources in the Carinae nebula are at $(\alpha, \delta) = (10^{\text{h}}44^{\text{m}}, -59.64^\circ)$ and $(10^{\text{h}}33^{\text{m}}, -57.95^\circ)$ in J1994 coordinates. The mean signals from them are (9.0 ± 0.3) and (4.2 ± 0.1) mK in our beam, respectively, with the errors representing only the statistical uncertainty. The first source was also used as a pointing reference.

The statistical error on the determination of the average gain is 5%. Our estimates of possible systematic effects are at the level of $< 20\%$. We therefore adopt a gain uncertainty of 20%.

5. Analysis

The data analysis presented here differs slightly from that used for the previously reported PyI results; using the new method does not significantly change those results. We describe here the new method, which is used to arrive at all the results in this paper.

The output of each detector is sampled at 100 Hz and demodulated in software, synchronously with the motion of the chopping flat. Two lockin demodulations are used; one (the “optical phase”) is maximally sensitive to the 3-beam signal from the sky, while the second (the “quadrature phase”) is shifted by 90° from the optical phase and should have no response to a stationary sky signal. We confine our discussion to the optical phase data, giving results from the quadrature phase where relevant.

Within each of the 42 stares in a scan, the mean and variance $\sigma_{S_j}^2$ of the lockin values are calculated. The means are then combined in a pairwise fashion into 4-beam values ΔT_j^k as described above, and an average variance σ_S^2 is calculated from the 42 values of $\sigma_{S_j}^2$. Thus σ_S^2 is a measure of the noise which contains drifts only within 10 to 30 second long stares.

As previously described, each channel measures a 4-beam value ΔT_j^k three times in succession ($k = 1, 2, 3$) for seven sky positions j . From these we find a mean for each channel at each position j , and an average error on those means, σ_m . Drifts up to the time separating observations of successive 4-beam positions (roughly 3 minutes), are included in σ_m . The variance from a celestial signal does not contribute to σ_m , and σ_m can therefore be used as an unbiased statistic for cutting scans.

The noise estimates described above are calculated for each channel in every complete scan. We use σ_S and σ_m , normalized to a “stare” duration of 30 seconds, on a channel by channel basis to remove scans which have been contaminated by excessive noise. The first cut removes scans with σ_S greater than 1.5 times the peak of its distribution. This procedure removes 20 to 25% of the scans for each channel in PyI, and 5 to 10% of those in PyII. The second cut removes scans with high values of σ_m ; the value at which scans are cut is placed so as to minimize the average final errorbar in the binned data. This step removes 19 to 27% of the scans for PyI, and 4 to 5% of those in PyII. The cuts remove more PyI data than PyII because of the poorer weather during that season. In all, approximately 50

hours (depending on the channel) of PyI data passed the cuts. For PyII, roughly 24 hours of data on the overlapping field (Field A), and 9 hours on the interleaving field (Field B) remained after the cuts.

The average value of σ_S from all scans that pass the cuts is a good indicator of chopped detector noise. For PyI, the noise in the four channels is 2.5, 2.9, 2.1 and 1.9 mK $\cdot\sqrt{s}$; For the three operational channels of PyII, it is 2.1, 1.3 and 5.7 mK $\cdot\sqrt{s}$. These values are in good agreement with those found from the quadrature values of both σ_S and σ_m . The optical phase value of σ_m is higher (for the sensitive channels), due to atmospheric contamination. For PyI it is 4.1, 4.2, 4.0 and 3.9 mK $\cdot\sqrt{s}$; for PyII these values are 2.9, 2.7 and 5.6 mK $\cdot\sqrt{s}$.

For sky positions observed by more than one channel, the 4-beam averages from neighboring channels are combined into a single value within a scan by forming a weighted average of the left and right-hand channels. The average value of $1/\sigma_S^2$ over all uncut scans is used as the weight. If one of the channels is cut by the previously described procedures, its neighbor is cut as well.

After this treatment, a statistical mean and error are calculated from the uncut scans at each of the sky positions j . The errors are within 10% of those expected given the distribution of σ_m , indicating there is little if any additional atmospheric contamination. These means and errors, after multiplying by 1.07 to correct for the estimated atmospheric absorption in our band, are the final values and errors for the 4-beam temperature differences on the sky.

6. Results

The results of the analysis of the PyI data and of the overlapping portion (Field A) of the PyII data set appear in Figure 1. The agreement is good; taking the difference of the two data sets [$(\text{PyI} - \text{PyII})/2$] gives a result that agrees well with zero signal (reduced $\chi^2 \equiv \chi_\nu^2 = 12./15$). The weighted mean of the two data sets is shown as the filled circles in Figure 2; here the agreement with zero signal is very poor ($\chi_\nu^2 = 191./16$). The contrast between the χ^2 's for the summed and differenced data sets indicates that the signal in the two data sets is the same.

A set of patches (Field B) that interleaves those from Field A was also observed during the PyII season. The locations of the Field B beams are found by moving one half of a chopper throw in negative right ascension (1.38° on the sky) from the beams that make up

Field A. Analyzing the Field B data leads to the values shown as open squares in Figure 2. Less time was spent observing this field, and the errors are larger than on Field A. The agreement with zero sky signal is good for Field B ($\chi^2_\nu = 14./15$).

The results shown in Figure 2 were measured in a single frequency band, so we cannot spectrally discriminate between CMBR anisotropies and the various possible foregrounds. In Paper I we discussed the expected levels of galactic foreground contamination, which are smaller than the signals seen. Proceeding under the assumption that these signals represent fluctuations in the CMBR, we multiply the values plotted in Figure 2 by 1.24 to convert them from Rayleigh-Jeans temperature units to temperature differences in a 2.73 K blackbody, and use the integrated likelihood function to form confidence interval estimates for the sky signal in two models with Gaussian CMBR fluctuations. For both analyses we use the full correlation matrix including off-diagonal elements describing correlations present because of the theoretical model and those induced by the observing strategy.

The first model consists of a sky with a Gaussian autocorrelation function (GACF) with a coherence angle of $\theta_c = 1^\circ$. We set limits on $\sqrt{C_0}$, the rms amplitude of the fluctuations in $\Delta T/T$. The uncertainty in beamwidth leads to less than a 2% error in $\sqrt{C_0}$. The GACF limits can be converted to an estimate of the flat band power sampled by our window function. Following the recipe of Bond 1994, we find for our window function, $\Delta T_{Band\ Power} = 0.73\Delta T_{GACF}$. The effective center of our window function for a flat band power spectrum lies at $\ell_e = 93$.

We also use a model with an uncorellated sky, $C(\theta) = \delta(1 - \cos\theta)$, to find the rms of our data set, from which we derive another band power estimate. Correlations due to beam overlap are less than 1%, and we ignore them. This analysis gives results that are within a few percent of those found by converting the GACF limits, indicating that the flat band power is insensitive to the form of the corellation function used in the likelihood calculation.

The results for the various combinations of data sets and analyses are given in Table 1. The confidence intervals quoted in the table do not include the 20% calibration error. The first four entries in Table 1 show that the signal seen in the first season appears again in the second. The last entry in Table 1 gives our final result using the data from both seasons and both fields.

7. Conclusions

After detecting a signal in our first year of observations, we re-observed the same portion of the sky and detected the same signal. This provides further evidence that the signal is celestial rather than systematic in nature.

Additionally, an interleaving set of spots was observed during the second season. Likelihood analyses on the entire data set are used to derive two estimates of the sky signal. First, we find $79_{-19}^{+28}\mu\text{K}$ for the total sky rms for a Gaussian autocorrelation model with a coherence angle of 1° . Second, we find a band power of $57_{-14}^{+20}\mu\text{K}$, using an autocorrelation function given by $C(\theta) = \delta(1 - \cos \theta)$. The stated errors are 1σ limits that include the 20% calibration uncertainty added in quadrature with the likelihood-derived errors.

We thank the Antarctic Support Associates staff at the South Pole for making a successful season possible, and Ted Griffith, Bob Pernic, and Bill Vinje for valuable assistance there. This research was supported by the James S. McDonnell Foundation, PYI grant NSF AST 90-57089, and the National Science Foundation under a cooperative agreement with the Center for Astrophysical Research in Antarctica (CARA), grant NSF OPP 89-20223. CARA is an NSF Science and Technology Center. JR was supported by the McCormick Fellowship at the University of Chicago.

| Dataset | Field | Band Power | GACF |
|---------------|-------|--|---|
| | | $T_0\sqrt{\ell_e(\ell_e + 1)C_\ell/(2\pi)}$ $\ell_e = 93$ | $T_0\sqrt{C_0}$ $\theta_c = 1^\circ$ |
| PyI | A | 66_{-11}^{+27} | 90_{-15}^{+36} |
| PyII | A | 68_{-11}^{+32} | 91_{-15}^{+42} |
| (PyI&PyII) | A | 69_{-10}^{+27} | 93_{-13}^{+36} |
| (PyI-PyII)/2. | A | (3, 19) | (5, 26) |
| PyII | B | (16, 59) | (23, 81) |
| (PyI&PyII) | A&B | 57_{-8}^{+16} | 79_{-10}^{+23} |

Table 1: Results of likelihood analyses.

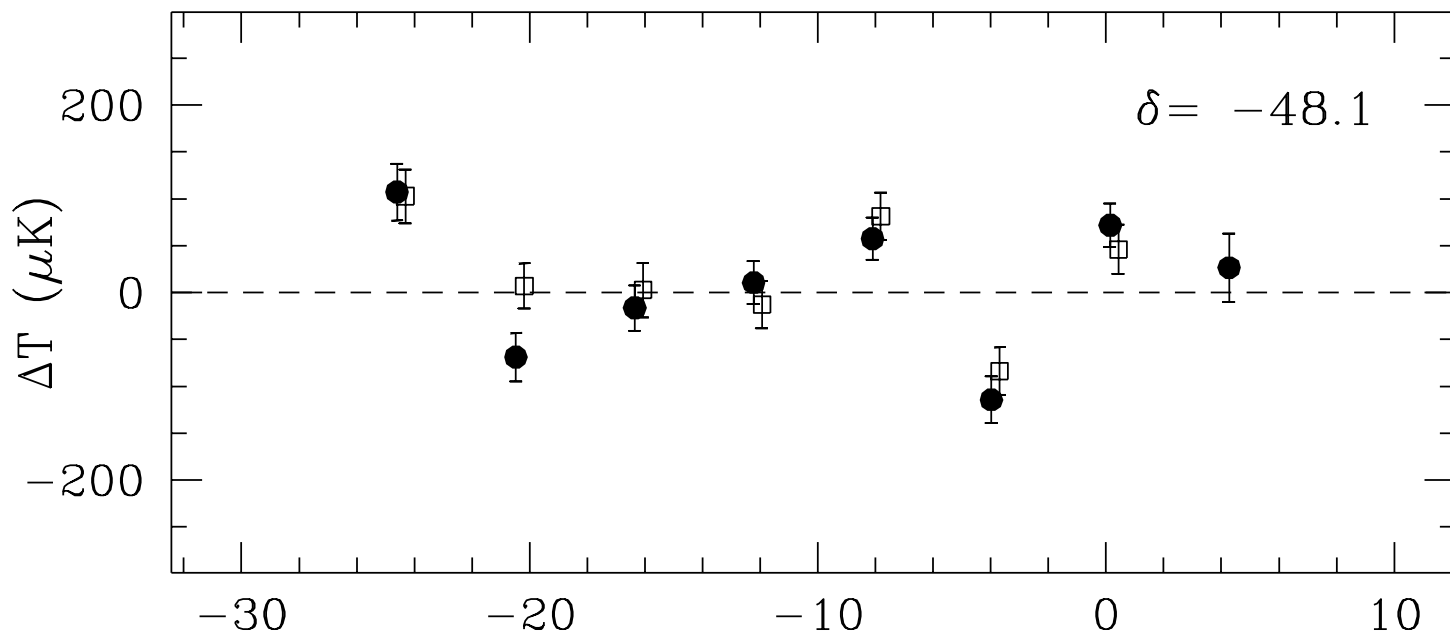
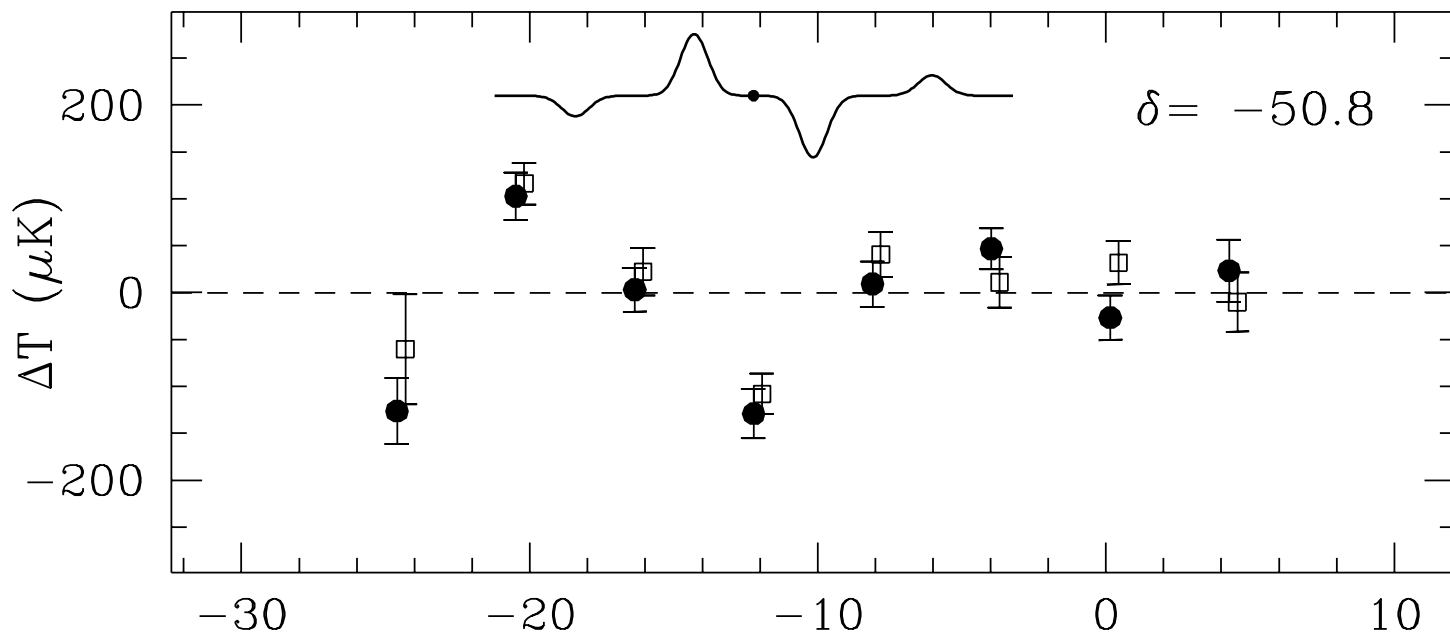
Values are in units of μK . Detections are quoted at the maximum in the likelihood, with 16% of the integrated likelihood above the upper errorbar, and 16% of the integrated likelihood below the lower one. For datasets with no significant detection, the value which maximizes the likelihood is given, along with a 95% upper limit from the integrated likelihood. The 20% calibration uncertainty is not included in these errors. The signals from the dark channel and from the quadrature phase are consistent with zero.

REFERENCES

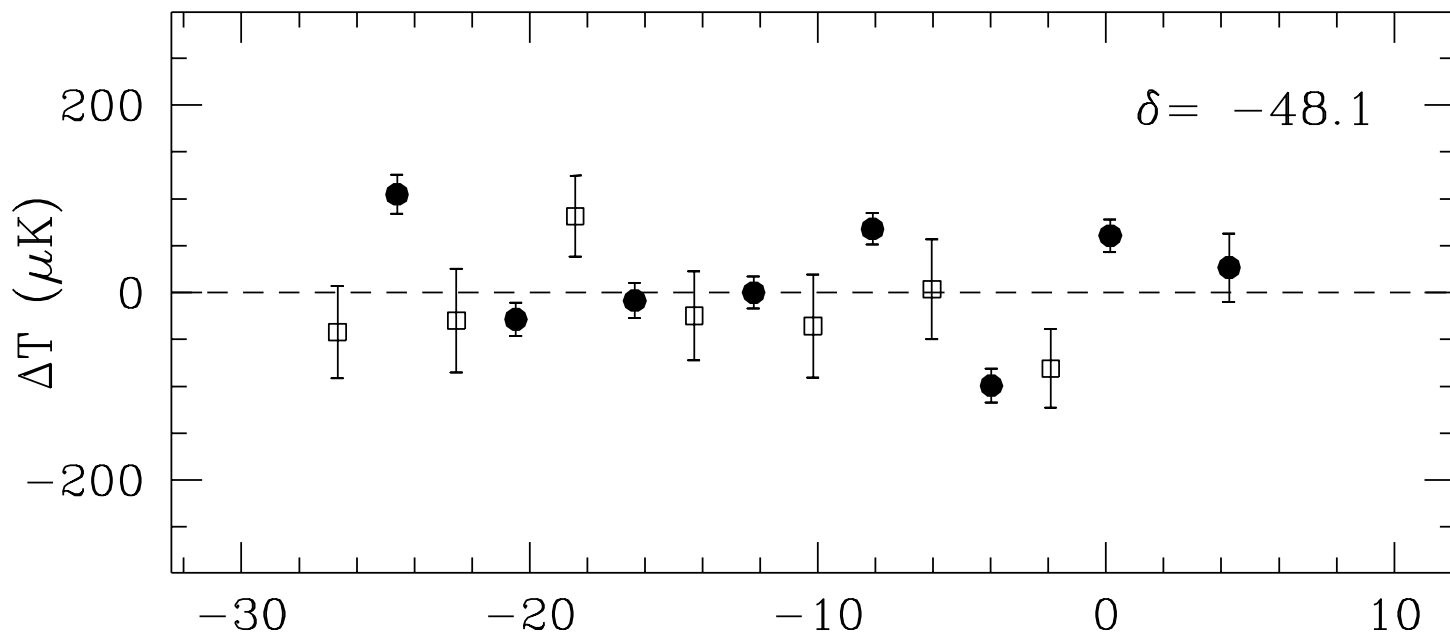
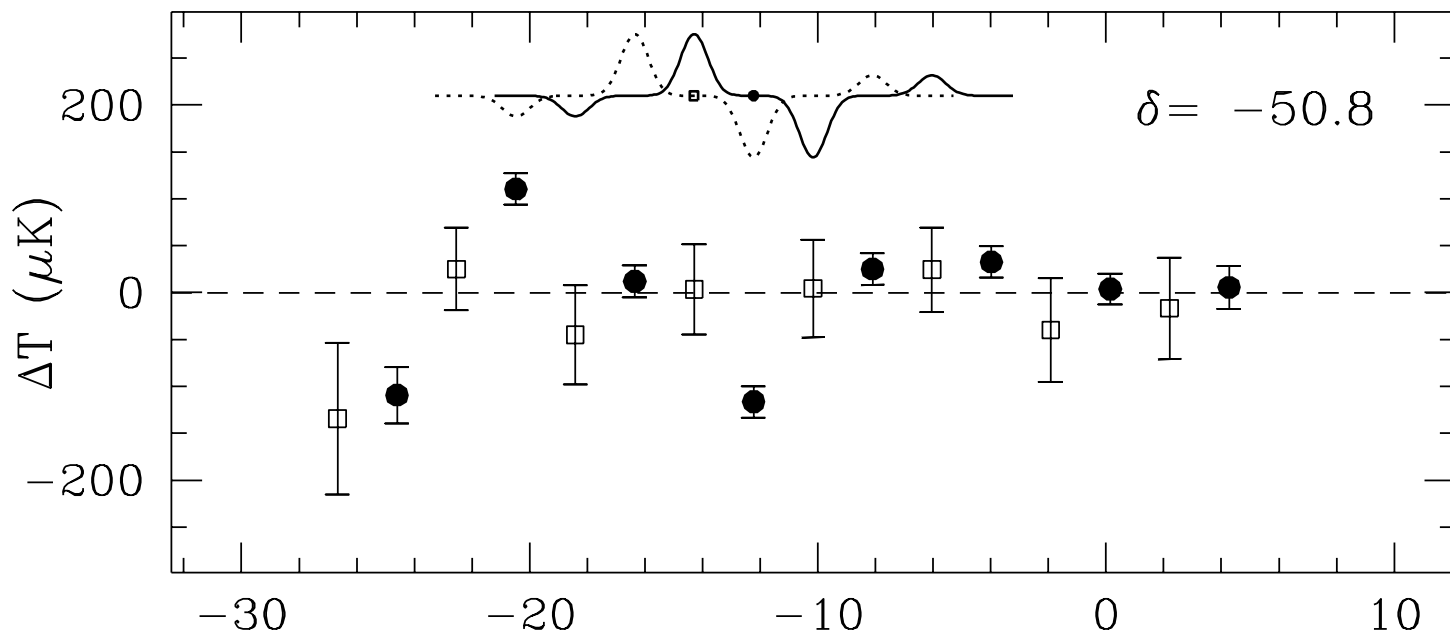
- Bennett, C. L. *et al.* 1994, ApJ **436** 423
- Bond, J. R., CITA-94-5, astro-ph/9402043, *preprint*.
- Cheng, E. S. *et al.* 1994, ApJ **422**, L37
- de Bernardis, P. *et al.* 1994, ApJ **422**, L33
- Devlin, M. J. *et al.* 1994, ApJ **430**, L1
- Dragovan, M., Ruhl, J. E., Novak, G., Platt, S. R., Crone, B., Pernic, R., and Peterson, J. B., 1994, ApJ **427** L67
- Ganga, K., Cheng, E., Meyer, S., and Page, L., 1993, ApJ **410** L57
- Gundersen, J. O. *et al.* 1995, ApJ **443** L57
- Netterfield, C. B., Jarosik, N., Page, L., Wilkinson, D., and Wollack, E., 1995, ApJ **445** L69
- Ruhl, J. E. 1993, Ph.D. thesis, Princeton University
- Ruhl, J. E. and Dragovan, M. 1992, in *Low Temperature Detectors for Neutrinos and Dark Matter*, Vol. 4, ed. N. E. Booth and G. L. Salmon, (Editions Frontieres), p. 461
- Ruhl, J. E., Dragovan, M., Novak, G., Platt, S. R., and Crone, B. K., 1995, in the Proceedings of the Capri CMB Workshop, Astrophys. Lett. & Comm., in press
- White, M., Scott, D., Silk, J., 1994, ARA&A **32** 319

Fig. 1.— Results from PyI and PyII for Field A. The PyI results are plotted as the solid circles, and the PyII results are shown as the open squares. They are offset horizontally for clarity. The 4-beam response pattern is shown in the top panel, aligned with the point plotted at $\alpha = -12^\circ$. The temperature axis is plotted in Rayleigh-Jeans units; to convert to thermodynamic temperature differences for a 2.73 K blackbody, multiply by 1.24.

Fig. 2.— Final results for both fields. The weighted mean of PyI and PyII for Field A are shown as the solid circles. The open squares show the results of the observations of Field B done during the PyII season. The temperature axis is plotted in Rayleigh-Jeans units; to convert to thermodynamic temperature differences for a 2.73 K blackbody, multiply by 1.24.



Right Ascension (degrees)



Right Ascension (degrees)